

Measuring intermediate mass black hole binaries with advanced gravitational wave detectors

John Veitch,¹ Michael Pürrer,² and Ilya Mandel^{1,3}

¹*School of Physics and Astronomy, University of Birmingham, Birmingham, B15 2TT, United Kingdom*

²*School of Physics and Astronomy, Cardiff University, Cardiff, CF24 3AA, United Kingdom*

³*Monash Center for Astrophysics, Monash University, Clayton, VIC 3800, Australia*

We perform a systematic study to explore the accuracy with which the parameters of intermediate-mass black hole binary (IMBHB) systems can be measured from their gravitational wave (GW) signatures using second-generation GW detectors. We make use of the most recent reduced-order models containing inspiral, merger and ringdown signals of aligned-spin effective-one-body waveforms (SEOBNR) to significantly speed up the calculations. We explore the phenomenology of the measurement accuracies for binaries with total masses between 50 and 500 M_{\odot} and mass ratios between 0.1 and 1. We find that (i) at total masses below $\sim 200 M_{\odot}$, where the signal-to-noise-ratio is dominated by the inspiral portion of the signal, the chirp mass parameter can be accurately measured; (ii) at higher masses, the information content is dominated by the ringdown, and total mass is measured more accurately; (iii) the mass of the lower-mass companion is poorly estimated, especially at high total mass and more extreme mass ratios; (iv) spin cannot be accurately measured for our injection set with non-spinning components. Most importantly, we find that for binaries with non-spinning components at all values of the mass ratio in the considered range and at network signal-to-noise ratio of 15, analyzed with spin-aligned templates, the presence of an intermediate-mass black hole with mass $> 100 M_{\odot}$ can be confirmed with 95% confidence in any binary that includes a component with a mass of $130 M_{\odot}$ or greater.

PACS numbers: 04.30.Tv, 97.60.Lf

INTRODUCTION

Advanced LIGO [1] and Virgo [2] detectors are expected to start taking data in late 2015 and 2016 [3], respectively. Compact binary coalescences are a key source of gravitational-wave (GW) signals for advanced detectors [e.g., 4, 5]. These may include binaries where one or both components are intermediate-mass black holes (IMBHs), with mass in the ~ 50 — few hundred M_{\odot} range.

There is growing observational and theoretical evidence for the existence of IMBHs in globular clusters [see 6, for review]. Observational evidence comes in the form of observations of ultra-luminous X-ray sources (ULX), cluster dynamics (though these are mostly sensitive to higher-mass IMBHs, whose GW signatures would be at frequencies below the detectors' sensitive band), and, most recently, a tentative quasi-periodic oscillator observation of a 400 M_{\odot} IMBH [7]. On the theoretical side, a number of models have been predicted for IMBH growth, from direct collapse from very massive stars [e.g., 8] to runaway collision scenarios [9, 10] or gradual growth through stellar-mass BH mergers [e.g., 11] or accretion [12].

Advanced GW detectors could observe inspirals of stellar-mass compact-objects into IMBHs in globular clusters [13]. IMBH binary mergers are possible if the binary fraction in a globular cluster is sufficiently high to allow the formation of two IMBHs [14], or via mergers of two globular clusters with each other and subsequent coalescences of the IMBHs they host [15, 16]. Outside of globular clusters, merging compact binaries including IMBHs could form directly from isolated binaries com-

posed of very massive ($\gtrsim 300 M_{\odot}$) stars [17]. All of these scenarios could produce advanced-detector event rates of tens or more detections per year, though much lower rates are also possible. Meanwhile, future detectors with good low-frequency sensitivity, such as the proposed Einstein Telescope [18], could observe up to thousands of IMBH binary mergers per year [19] and use high-redshift IMBH binary observations to probe the history of massive black hole formation [20, 21].

GW observations, which allow for a direct mass measurement, could provide the first completely unambiguous proof of the existence of IMBHs in the few-hundred-solar-mass range. If such IMBHs are discovered, their observations would shed light on very massive star evolution and globular cluster dynamics. IMBHs could also prove to be particularly accurate probes of strong-field dynamical gravity, allowing for tests of the general theory of relativity [e.g., 22, 23]. As the coalescence of IMBHBs is expected to be electromagnetically quiet, gravitational waves are likely to be the only means of observing these systems directly. For this reason, the LIGO and Virgo collaborations have carried out searches for IMBH binaries in initial detector data (which did not yield detections) [24–26] and intend to do the same in the advanced detector era with more sensitive instruments. However, in order to establish that an IMBH has been detected and to explore the scientific consequences of this discovery, it is necessary to analyze the GW signature of a coalescence in order to infer the parameters of the systems, particularly the component masses. In this paper we perform the first systematic study of the accuracy of IMBHB mass

measurements achievable with GW observations.

Accurate models for GWs emitted from IMBH binaries must include the inspiral, merger, and ringdown phases of the coalescence. One of the most accurate available theoretical waveform families are effective-one-body (EOB) models [27–29]. EOB is an analytical approach that combines post-Newtonian expansion, re-summation techniques and perturbation theory with additional calibration of certain model parameters against waveforms obtained by numerically integrating Einstein’s equations on supercomputers. These models are defined via a complicated set of ordinary differential equations in the time-domain and can be very computationally expensive to generate, limiting their use in parameter estimation studies to date. Novel reduced order modeling (ROM) techniques [30–32] have allowed for the construction of fast and accurate surrogate models of EOB waveforms. In particular, we use the frequency domain ROMs [31, 32] for EOB waveforms with spins aligned with the orbital angular momentum of the binary, defined in [33, 34] and implemented in LAL [35]. This allows us to perform simulations on a scale unprecedented for this class of sources.

SIMULATIONS

We performed a systematic study of the accuracy with which the masses and spins of the IMBHB could be recovered from GW observations by Advanced LIGO and Advanced Virgo GW detectors operating at design sensitivity. For Advanced LIGO we used the zero-detuned, high-power detector configuration [36], and for Advanced Virgo a phenomenological fit to the design sensitivity curve [37], both of which are displayed in Figure 1 along with typical characteristic signal amplitudes. For our analysis we began generating the waveforms at a lower frequency of 10 Hz in both LIGO and Virgo instruments, allowing us to take full advantage of the low-frequency sensitivity of the instruments, which will be achieved toward the end of the decade. The use of zero-noise mock data sets to estimate parameter measurement accuracy relies on the assumption that the noise is stationary and Gaussian; although Berry et al. [38] demonstrated that non-stationary realistic noise does not significantly influence parameter estimation for neutron star binaries, departures from stationarity (noise “glitches”) could play a larger role for low-frequency, short-duration IMBHB signals.

To investigate parameter measurement accuracy, we analyzed a set of mock data sets (injections) with the **LALInference** [39] Bayesian parameter-estimation pipeline. This pipeline returns a set of samples from the joint posterior distribution for the signal parameters. We can readily convert this output into the innermost 90% credible region, spanning from the 5th to the 95th percentile, on marginalized single-parameter posterior

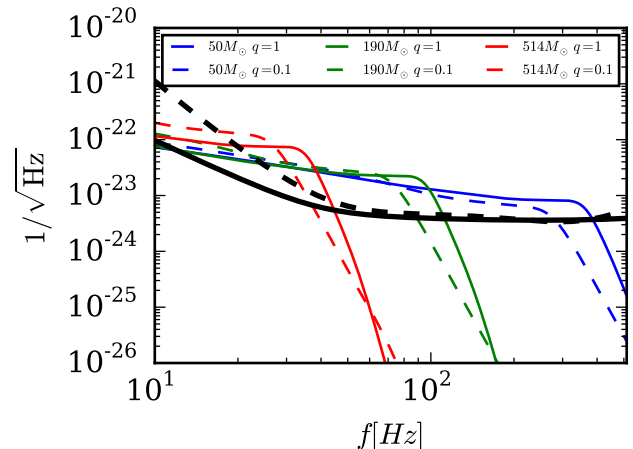


Figure 1: Characteristic amplitudes $h_c \equiv \sqrt{f}|\tilde{h}(f)|$ of SEOBNRv2 [34] injections with various total masses and mass ratios, at network SNR 15 used in this study. In black, the detector noise amplitude spectrum $\sqrt{S_n(f)}$ of the Advanced LIGO design noise-curve (solid) and the Advanced VIRGO noise-curve (dashed).

distributions, which we use as a proxy for measurement accuracy. We find this to be a more robust metric for measurement accuracy than the standard deviation of the highly non-Gaussian posteriors.

We injected data with both SEOBNRv1 and SEOBNRv2 [34] waveforms, and used corresponding single-spin ROM template families for recovery. We found resulting measurement accuracies that are qualitatively and quantitatively similar, so we only show results from the more recent SEOBNRv2 model here. We included only the dominant $l = m = 2$ mode of the gravitational wave signal in our simulations, as this is the only mode included in the SEOBNRv2 reduced order model. This omission means that our results can only serve as a conservative estimate of the parameter estimation performance for IMBHB systems, since the higher frequency harmonics of the signal can carry information to further constrain the signal model, especially at high masses [40–42]. Further development of ROMs to include both higher harmonics and spin is necessary to provide timely results with the best possible accuracy. We did not include the cosmological redshift of the waveforms, so our results should be interpreted as measurements of the redshifted masses in the rest frame of the detectors.

In order to explore measurement accuracy as a function of mass and mass ratio, we carried out injections for a broad range of total masses $M_{\text{total}} = m_1 + m_2$ between 50 and 500 M_\odot , where $m_1 > m_2$ are the component masses. For each mass, we injected systems at four mass ratios $q = m_2/m_1$ of 1, 1/2, 1/4 and 1/10, always with non-spinning components. All simulated signals were oriented

such that the orbital angular momentum vector was inclined at 30° to the line of sight between the Earth and the binary. Although the orientation and sky location were the same in all simulations, we do not expect the measurement of the mass and aligned spin parameters to be significantly affected by this choice, since we do not include higher modes which can couple mass ratio measurement to extrinsic parameter accuracy [42]. The distance was chosen to yield a constant coherent signal-to-noise ratio (SNR) of 15.

For the Bayesian analysis, we used flat priors on the component masses within the range $m_1, m_2 \in [5, 1000] M_\odot$, limited the total mass to $M_{\text{total}} \leq 1000 M_\odot$, and limited the mass ratio $m_2/m_1 \geq 0.01$. We did not assume any of the source parameters were known when performing parameter estimation, allowing an isotropic prior on orientation, and a uniform-in-volume prior on binary location out to a luminosity distance of 15 Gpc (a redshift of ~ 1.9). The prior on the single aligned spin χ was fixed to be flat in $[-1, 0.6]$, the range of validity of the SEOBNRv1 [33] approximant. Since this prior distribution does not match the distribution of sources analyzed, we should anticipate that posteriors on individual injections can be centered away from the true values, despite the self-consistency of **LALInference**, which has been demonstrated to produce $X\%$ credible intervals that contain the true value $X\%$ of the time [38, 39, 43]. For example, the low *a priori* probability of high-mass extreme-mass ratio injections with non-spinning components, coupled to the asymmetry in the impact of remnant spin on the well-measured central frequency of the dominant ringdown harmonic [e.g., 44], will lead to a typical over-estimate of the inferred total mass for such sources. This is compounded by the prior on distance $p(d_L) \propto d_L^2$, which for a fixed amplitude tends to prefer higher mass sources at greater distances.

RESULTS

Mass measurement Figure 2 shows the 90% credible interval for the chirp mass, $\mathcal{M} = m_1^{3/5} m_2^{3/5} M_{\text{total}}^{-1/5}$, as a function of the total mass M_{total} .

At lower masses, the signal is dominated by the ‘chirping’ inspiral portion, and the phase evolution is a function of \mathcal{M} at leading order, which is therefore the most strongly constrained parameter when analysing lower mass systems [45]. We find that the width of the 90% credible interval on \mathcal{M} is $0.3 - 0.5 M_\odot$ at $M_{\text{total}} = 50 M_\odot$ and $0.7 - 3.5 M_\odot$ at $M_{\text{tot}} = 100 M_\odot$. For comparison, the same interval is typically $\lesssim 0.01 / 0.03 / 0.1 M_\odot$ for binary neutron star systems / neutron star – black hole binaries / stellar-mass binary black holes, respectively [e.g., 45–47].

Meanwhile, as the mass increases, the inspiral moves to progressively lower frequencies and out of the sensitive band of the detector (see Figure 1) and the merger and

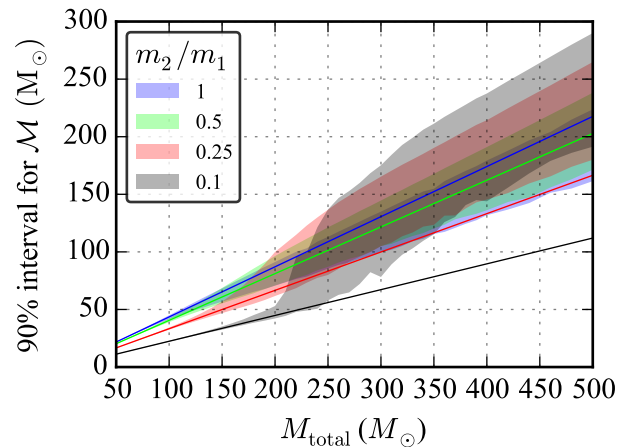


Figure 2: The 90% credible intervals for the chirp mass \mathcal{M} as a function of total mass M_{total} , for four mass ratios m_2/m_1 . True values are indicated by the solid lines. As M_{total} increases in the range $50 - 200 M_\odot$, the measurement of \mathcal{M} becomes steadily worse as the inspiral portion of the signal moves out of the sensitive band of the detector.

ringdown contribute an increasing fraction of the SNR (see Figure 3). At masses above $\sim 100 M_\odot$, the SNR is dominated by the merger and ringdown, and above $\sim 200 M_\odot$, by the ringdown. The ringdown frequency depends only on the total mass and spin of the merger product (the latter is a function of the mass ratio for non-spinning components). We therefore expect the total mass of high-mass systems to be better constrained than the chirp mass [this has previously been pointed out by Graff, Buonanno, and Sathyaprakash in ref. 48]; moreover, the accuracy of the M_{total} measurement should become increasingly insensitive to the mass ratio. Indeed, this is the behavior we see in Fig. 4, which shows the 90% credible interval for the total mass.

Alternatively, the mass measurement accuracy can be visualized by considering the 90% credible region widths on component masses. Figure 5 shows that component masses are generally harder to measure because of the significant uncertainty in the mass ratio typical for GW parameter estimation [45]. The mass of the lower-mass component m_2 is particularly poorly constrained, especially at high masses and more extreme mass ratios, where only the total mass is encoded in the ringdown signature. The fractional uncertainty of the better-measured m_1 component varies between 40% and 10% between M_{total} 100 and $300 M_\odot$.

Spin All of our injections have non-spinning components, and the SEOBNRv2ROM waveform model which we used includes only a single spin parameter $\chi = (m_1 \chi_1 + m_2 \chi_2)/M$, a combination of the dimen-

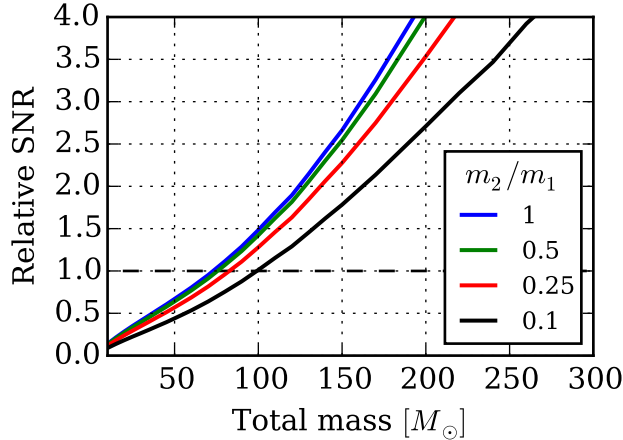


Figure 3: The relative SNR, the ratio of the SNR above and the SNR below the GW frequency at the innermost stable circular orbit (ISCO). We use the Schwarzschild ISCO $f_{\text{ISCO}} = 6^{-3/2}/(\pi M)$ which is strictly speaking only valid in the test particle limit. The relative SNR w.r.t. the ISCO depends on the mass-ratio. In contrast, the ratio of SNRs above and below half the ringdown frequency of each system is only weakly dependent on the mass ratio and reaches unity at a total mass of $150 M_{\odot}$.

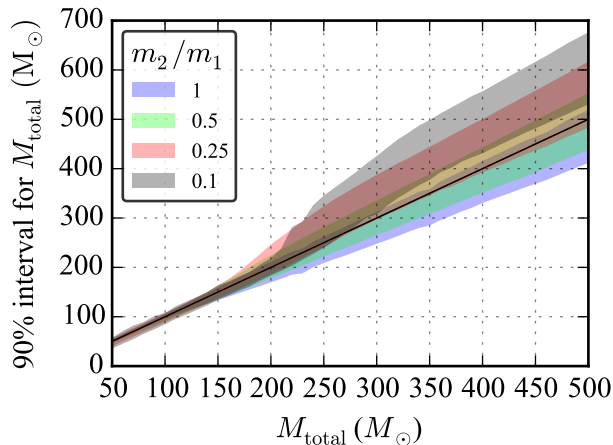


Figure 4: The 90% credible intervals for M_{total} .

sionless spins $\chi_i = \vec{L} \cdot \vec{S}_i / m_i^2$ aligned with the orbital angular momentum \vec{L} that plays a dominant role in governing the inspiral phase evolution through spin-orbit coupling [49, 50]. Figure 6 shows that the measurement accuracy of χ decreases with total mass, as the inspiral moves out of the detector band. In general, χ is not well constrained for non-spinning injections ($\chi = 0$), as χ values between ~ 0.2 and ~ -0.5 are allowed, spanning about half of the prior range $[-1, 0.6]$.

Measurability of parameters as a function of signal-to-noise ratio We also performed a series of simulations where we increased the signal-to-noise ratio from 5 to 100. The shape of the posterior probability density function approaches a multivariate Gaussian at high SNR; once this happens, we expect uncertainties on individual parameters to fall off as SNR^{-1} . As shown in Figure 7 this is indeed the case for SNRs larger than ~ 15 .

DISCUSSION

A key question that will arise when a massive system is detected is whether we can confidently establish that the system contains an IMBH. As the coalescence of IMBHB systems is likely to be electromagnetically quiet, GW observations will be essential to measuring the parameters of these systems. Our results indicate that advanced GW detectors, using models which include inspiral, merger and ringdown, will be able to constrain the masses of detected IMBHBs, at least under the assumption of aligned spins. Figure 8 shows the 5% lower bound on the mass of the more massive component m_1 as that parameter increases. This indicates that, at a network SNR of 15 or greater, the accuracy of inference will be sufficient to determine at 95% confidence that a system with non-spinning components does indeed contain an intermediate mass black hole with mass $> 100 M_{\odot}$ when the mass of at least one component is $\sim 130 M_{\odot}$ or greater.

The SEOBNR reduced order models [31, 32] have proven to be instrumental for performing systematic parameter estimation studies with SEOBNR waveforms and provide speedups of up to several orders of magnitude. At the high total masses and low sampling rate used in this study time-domain SEOBNR waveforms are comparatively quick to generate, but the speedup gained from ROM is still very significant. A single waveform evaluation with the ROMs is roughly 700 times faster than the likelihood computed from the time-domain SEOB-NRv2 model. Due to overhead costs the overall runtime of the simulations is roughly a factor 50 cheaper than with time-domain SEOBNR waveforms, allowing parameter estimation on sub-day timescales. As the waveform models improve further we will be able to analyse a broader range of physical effects, including higher harmonics, with the rapidity the ROMs provide.

JV was supported by STFC grant ST/K005014/1. MP was supported by STFC grant ST/I001085/1. IM acknowledges STFC support and the hospitality of the Monash Center for Astrophysics, supported by a Monash Research Acceleration Grant (PI Y. Levin). We thank Mark Hannam and Jonathan Gair for useful discussions.

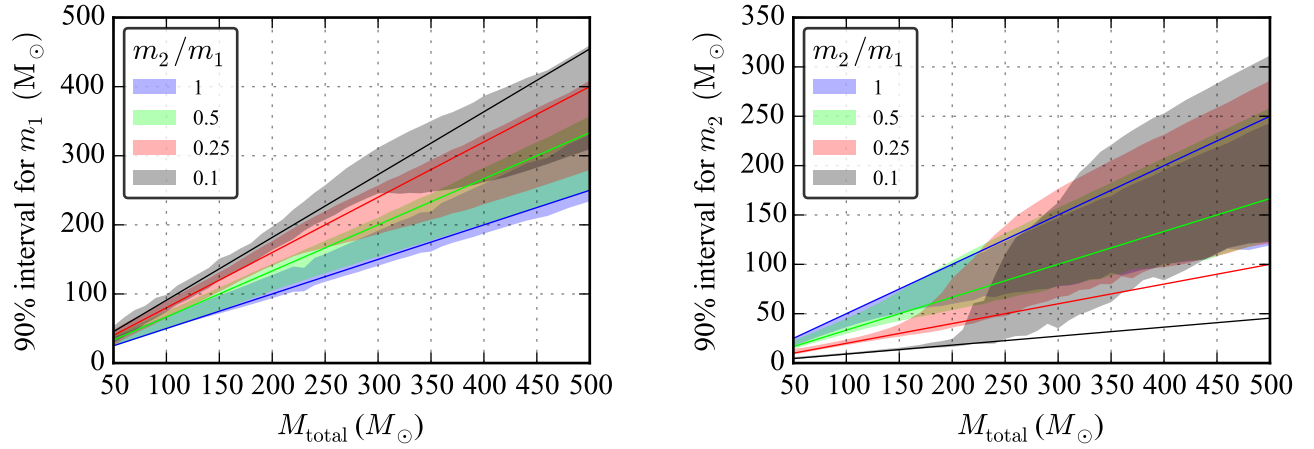


Figure 5: The 90% credible intervals for the component masses m_1 (left, larger companion) and m_2 (right, smaller companion).

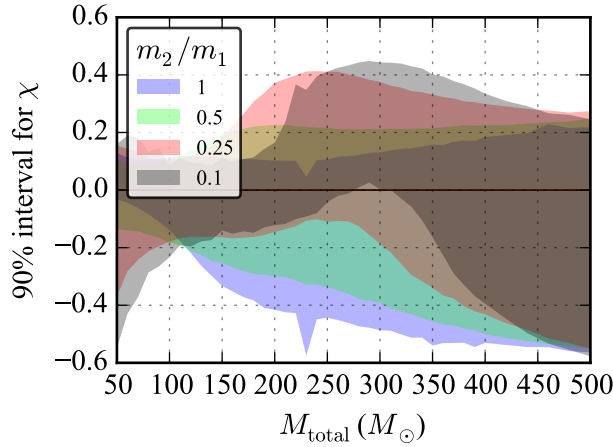


Figure 6: The 90% credible interval for the effective dimensionless spin χ .

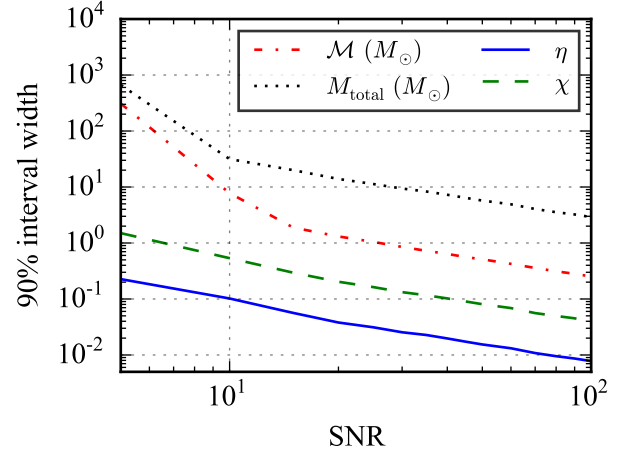


Figure 7: The width of the 90% credible intervals in chirp mass \mathcal{M} , total mass M_{total} , symmetric mass-ratio η and spin χ as a function of network SNR for mass-ratio $q = 0.25$ and total mass $100 M_{\odot}$.

[1] Harry, G. M. and the LIGO Scientific Collaboration, *Classical and Quantum Gravity* **27**, 084006 (2010).
[2] Virgo Collaboration, Virgo Technical Report VIR-0027A-09 (2009), <https://tds.ego-gw.it/itf/tds/file.php?callFile=VIR-0027A-09.pdf>.
[3] LIGO Scientific Collaboration, Virgo Collaboration, J. Aasi, J. Abadie, B. P. Abbott, R. Abbott, T. D. Abbott, M. Abernathy, T. Accadia, F. Acernese, et al., *ArXiv e-prints* (2013), 1304.0670.
[4] J. Abadie et al. (LIGO Scientific Collaboration and Virgo Collaboration), *Class. Quantum Grav.* **27**, 173001 (2010).
[5] I. Mandel and R. O'Shaughnessy, *Classical and Quantum Gravity* **27**, 114007 (2010), 0912.1074.
[6] M. C. Miller and E. J. M. Colbert, *International Journal of*

Modern Physics D **13**, 1 (2004), arXiv:astro-ph/0308402.
[7] D. R. Pasham, T. E. Strohmayer, and R. F. Mushotzky, *Nature* **513**, 74 (2014).
[8] P. Madau and M. J. Rees, *Astrophysical Journal* **551**, L27 (2001).
[9] S. F. Portegies Zwart and S. L. W. McMillan, *Astrophysical Journal* **576**, 899 (2002), astro-ph/0201055.
[10] S. F. Portegies Zwart, H. Baumgardt, P. Hut, J. Makino, and S. L. W. McMillan, *Nature* **428**, 724 (2004), arXiv:astro-ph/0402622.
[11] R. M. O'Leary, F. A. Rasio, J. M. Fregeau, N. Ivanova, and R. O'Shaughnessy, *Astrophysical Journal* **637**, 937 (2006), astro-ph/0508224.
[12] E. Vesperini, S. L. W. McMillan, A. D'Ercole, and

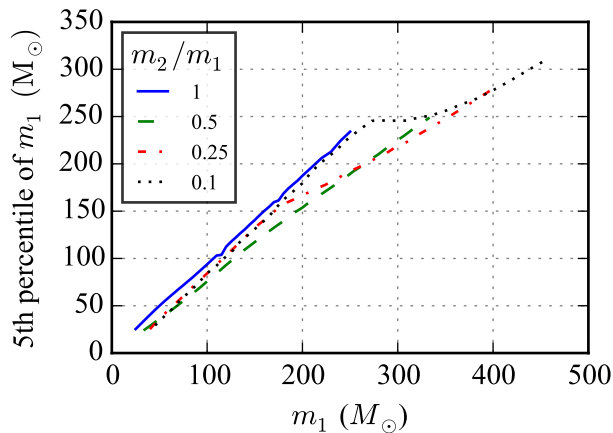


Figure 8: The 95%-confidence lower bound on the mass of the more massive component m_1 as a function of m_1 , showing that a system can be confidently classified as containing an IMBH with mass $> 100 M_\odot$ when m_1 exceeds $\sim 130 M_\odot$.

- F. D'Antona, *Astrophysical Journal* **713**, L41 (2010), 1003.3470.
- [13] I. Mandel, D. A. Brown, J. R. Gair, and M. C. Miller, *Astrophysical Journal* **681**, 1431 (2008), 0705.0285.
- [14] J. M. Fregeau, S. L. Larson, M. C. Miller, R. O'Shaughnessy, and F. A. Rasio, *Astrophysical Journal Letters* **646**, L135 (2006), astro-ph/0605732.
- [15] P. Amaro-Seoane and M. Freitag, *Astrophysical Journal* **653**, L53 (2006), astro-ph/0610478.
- [16] P. Amaro-Seoane and L. Santamaría, *Astrophysical Journal* **722**, 1197 (2010), 0910.0254.
- [17] K. Belczynski, A. Buonanno, M. Cantiello, C. L. Fryer, D. E. Holz, I. Mandel, M. C. Miller, and M. Walczak, *Astrophysical Journal* **789**, 120 (2014), 1403.0677.
- [18] M. Punturo, M. Abernathy, F. Acernese, B. Allen, N. Andersson, K. Arun, F. Barone, B. Barr, et al., *Classical and Quantum Gravity* **27**, 084007 (2010).
- [19] J. R. Gair, I. Mandel, M. C. Miller, and M. Volonteri, *General Relativity and Gravitation* **43**, 485 (2011), 0907.5450.
- [20] A. Sesana, J. Gair, I. Mandel, and A. Vecchio, *Astrophysical Journal* **698**, L129 (2009), 0903.4177.
- [21] J. R. Gair, I. Mandel, A. Sesana, and A. Vecchio, *Classical and Quantum Gravity* **26**, 204009 (2009), 0907.3292.
- [22] D. A. Brown, J. Brink, H. Fang, J. R. Gair, C. Li, G. Lovelace, I. Mandel, and K. S. Thorne, *Phys. Rev. Lett* **99**, 201102 (2007), arXiv:gr-qc/0612060.
- [23] C. L. Rodriguez, I. Mandel, and J. R. Gair, *Phys. Rev. D* **85**, 062002 (2012), 1112.1404.
- [24] J. Abadie, B. P. Abbott, R. Abbott, T. D. Abbott, M. Abernathy, T. Accadia, F. Acernese, C. Adams, R. Adhikari, C. Affeldt, et al., *Phys. Rev. D* **85**, 102004 (2012), 1201.5999.
- [25] The LIGO Scientific Collaboration, the Virgo Collaboration, J. Aasi, B. P. Abbott, R. Abbott, T. Abbott, M. R. Abernathy, T. Accadia, F. Acernese, K. Ackley, et al., *ArXiv e-prints* (2014), 1404.2199.
- [26] The LIGO Scientific Collaboration, the Virgo Collaboration, J. Aasi, B. P. Abbott, R. Abbott, T. Abbott, M. R. Abernathy, F. Acernese, K. Ackley, C. Adams, et al., *ArXiv e-prints* (2014), 1403.5306.
- [27] A. Buonanno and T. Damour, *Phys. Rev.* **D59**, 084006 (1999), gr-qc/9811091.
- [28] A. Buonanno and T. Damour, *Phys. Rev.* **D62**, 064015 (2000).
- [29] T. Damour, *Phys. Rev.* **D64**, 124013 (2001), gr-qc/0103018.
- [30] S. E. Field, C. R. Galley, J. S. Hesthaven, J. Kaye, and M. Tiglio, *Phys. Rev.* **X4**, 031006 (2014), 1308.3565.
- [31] M. Pürrer, *Class. Quant. Grav.* **31**, 195010 (2014), 1402.4146.
- [32] M. Pürrer, *ArXiv e-prints* (2015), 1512.02248.
- [33] A. Taracchini, Y. Pan, A. Buonanno, E. Barausse, M. Boyle, T. Chu, G. Lovelace, H. P. Pfeiffer, and M. A. Scheel, *Phys. Rev.* **D86**, 024011 (2012), 1202.0790.
- [34] A. Taracchini, A. Buonanno, Y. Pan, T. Hinderer, M. Boyle, et al., *Phys. Rev.* **D89**, 061502 (2014), 1311.2544.
- [35] LALSuite, The LIGO Scientific Collaboration, Lsc algorithm library (lal) – <https://www.lsc-group.phys.uwm.edu/daswg/projects/lalsuite.html>.
- [36] L. Barsotti and P. Fritschel, *Tech. Rep.* T1200307, The LIGO Scientific Collaboration and the Virgo Collaboration (2014), <https://dcc.ligo.org/LIGO-T1200307/public>.
- [37] A. Manzotti and A. Dietz, *ArXiv e-prints* (2012), 1202.4031, URL <http://adsabs.harvard.edu/abs/2012arXiv1202.4031M>.
- [38] C. P. L. Berry, I. Mandel, H. Middleton, L. P. Singer, A. L. Urban, A. Vecchio, S. Vitale, K. Cannon, B. Farr, W. M. Farr, et al., *Astrophysical Journal* **804**, 114 (2015), 1411.6934.
- [39] J. Veitch, V. Raymond, B. Farr, W. Farr, P. Graff, S. Vitale, B. Aylott, K. Blackburn, N. Christensen, M. Coughlin, et al., *Phys. Rev. D* **91**, 042003 (2015).
- [40] T. B. Littenberg, J. G. Baker, A. Buonanno, and B. J. Kelly, *Phys. Rev.* **D87**, 104003 (2013), 1210.0893.
- [41] V. Varma, P. Ajith, S. Husa, J. C. Bustillo, M. Hannam, et al., *Phys. Rev.* **D90**, 124004 (2014), 1409.2349.
- [42] P. B. Graff, A. Buonanno, and B. S. Sathyaprakash, *ArXiv e-prints* (2015), 1504.04766.
- [43] T. Sidery, B. Aylott, N. Christensen, B. Farr, W. Farr, F. Feroz, J. Gair, K. Grover, P. Graff, C. Hanna, et al., *Phys. Rev. D* **89**, 084060 (2014), 1312.6013.
- [44] E. Berti, V. Cardoso, and C. M. Will, *Phys. Rev. D* **73**, 064030 (2006), arXiv:gr-qc/0512160.
- [45] J. Aasi, J. Abadie, B. P. Abbott, R. Abbott, T. D. Abbott, M. Abernathy, T. Accadia, F. Acernese, C. Adams, T. Adams, et al., *Phys. Rev. D* **88**, 062001 (2013), 1304.1775.
- [46] C. L. Rodriguez, B. Farr, V. Raymond, W. M. Farr, T. B. Littenberg, et al., *Astrophys. J.* **784**, 119 (2014), 1309.3273.
- [47] I. Mandel, C.-J. Haster, M. Dominik, and K. Belczynski, *MNRAS* **450**, L85 (2015), 1503.03172.
- [48] P. Astone, A. Weinstein, M. Agathos, M. Bejger, N. Christensen, T. Dent, P. Graff, S. Klimenko, G. Mazzolo, A. Nishizawa, et al., *General Relativity and Gravitation* **47**, 11 (2015).
- [49] P. Ajith, *Phys. Rev. D* **84**, 084037 (2011), 1107.1267.
- [50] M. Pürrer, M. Hannam, P. Ajith, and S. Husa, *Phys. Rev.* **D88**, 064007 (2013), 1306.2320.